Large-Scale Covariability between Aerosol and Precipitation Over the 7-SEAS Region: Observations and Simulations

Jingfeng Huang[1,2,*], N. Christina Hsu[2], Si-Chee Tsay[2], Chidong Zhang[3], Myeong Jae Jeong[4], Ritesh Gautam[2,5], Corey Bettenhausen[2,6], Andrew M. Sayer[2,5], Richard A. Hansell[2,7], Xiaohong Liu[8], Jonathan H. Jiang[9]

[1] Morgan State University, Baltimore, MD, USA;

[2] NASA Goddard Space Flight Center, Greenbelt, MD, USA;

[3] University of Miami, Miami, FL, USA;

[4] Gangneung-Wonju National University, Gangneung, Korea.

[5] Universities Space Research Association, MD, USA

[6] Science Systems and Applications Inc., Lanham, MD, USA;

[7] University of Maryland, College Park, MD, USA

[8] Pacific Northwest National Laboratory, Richland, WA, USA

[9] NASA Jet Propulsion Laboratory, Pasadena, CA, USA;

[*] Corresponding Author

Tel/Fax: +1 301 614 6131 / +1 301 614 6307

E-mail address: jingfeng.huang@nasa.gov

Abstract

One of the seven scientific areas of interests of the 7-SEAS field campaign is to evaluate the impact of aerosol on cloud and precipitation (http://7-seas.gsfc.nasa.gov/). However, large-scale covariability between aerosol, cloud and precipitation is complicated not only by ambient environment and a variety of aerosol effects, but also by effects from rain washout and climate factors. This study characterizes large-scale aerosol-cloud-precipitation covariability through synergy of long-term multi-sensor satellite observations with model simulations over the 7-SEAS region [10S-30N, 95E-130E]. Results show that climate factors such as ENSO significantly modulate aerosol and precipitation over the region simultaneously. After removal of climate factor effects, aerosol and precipitation are significantly anti-correlated over the southern part of the region, where high aerosols loading is associated with overall reduced total precipitation with intensified rain rates and decreased rain frequency, decreased tropospheric latent heating, suppressed cloud top height and increased outgoing longwave radiation, enhanced clear-sky shortwave TOA flux but reduced all-sky shortwave TOA flux in deep convective regimes; but such covariability becomes less notable over the northern counterpart of the region where low-level stratus are found. Using CO as a proxy of biomass burning aerosols to minimize the washout effect, large-scale covariability between CO and precipitation was also investigated and similar large-scale covariability observed. Model simulations with NCAR CAM5 were found to show similar effects to observations in the spatio-temporal patterns. Results from both observations and

simulations are valuable for improving our understanding of this region's meteorological system and the roles of aerosol within it.

Key words: aerosol; precipitation; large-scale covariability; aerosol effects; washout; climate factors; 7-SEAS; CO; CAM5

1. Introduction

In recent decades, atmospheric aerosols have attracted increasing attention, in part owing to their relations to human activities and anthropogenic sources, air quality and environment sustainability, and corresponding climatic impact. However, a quantitative evaluation of global aerosol climatic effects still faces many hurdles and have large uncertainties (IPCC, 2007). Conceivably, a better understanding of large-scale covariability between aerosol and precipitation in aerosol 'hotspot' regions is needed as an important step towards their global evaluation.

Large-scale covariability between aerosol and precipitation consists of three components. The first component is the effect of precipitation on aerosol (wet deposition, a.k.a. the 'washout effect'). Washout always results in a negative linkage between aerosol loading and precipitation, because stronger or longer raining removes more aerosols from in the air. However, few studies have focused on the effectiveness of washout processes to answer questions such as what is the effective rain rate range that can wash out aerosols most efficiently. Imaging satellite sensors are still having difficulties in measuring aerosols in the presence of clouds, whereas ground measurements of aerosol depositions are still very limited and sparse. These all reinforce the need for studies to start documenting the observational evidences on aerosol-precipitation covariability.

The second component in the large-scale aerosol-precipitation covariability is aerosol effects on precipitation. It includes direct, semi-direct, and microphysical ('indirect') effects. The direct aerosol radiative effect is so-called because aerosol reflects or absorbs solar radiation and therefore directly perturbs the radiation budget, regional dynamics as well as large-scale climate system (Carlson and Benjamin 1980; Miller and Tegen 1998; Diaz et al. 2001; Ramanathan et al. 2001; Yoshioka et al. 2007). The semi-direct effect links aerosol absorption to cloud amount, through excess radiation absorbed by aerosols within clouds leading to faster evaporation of cloud water and in turn reducing cloud amount (Ackerman et al., 2000; Feingold et al., 2005). On the other hand, microphysical or 'indirect' effect emphasizes changes in cloud microphysics due to aerosols acting as cloud condensation nuclei (CCN) or ice nuclei (IN) and changing cloud droplet number and effective radius, cloud lifetime and precipitation efficiency (Twomey et al. 1984; Albrecht 1989; Sassen et al. 2003; Lohmann and Feichter 2005). Model simulations from Ackerman et al. (2000) found that mid-tropospheric radiative heating from smoke absorption stabilized the lower troposphere and reduced cloudiness. Koren et al. (2004) and Feingold et al. (2005) through observations and simulations respectively also demonstrated that cloud fraction decreased over Amazon in response to higher aerosol optical thickness (AOT) that increased tropospheric solar absorption and radiation warming. It is intriguing to explore how the cloud systems in tropical Asia, as another aerosol hotspot, may respond to aerosol effects.

The third component in the aerosol-precipitation covariability is mediated by climate factors such as the El Niño-Southern Oscillation (ENSO) and meteorological factors such as water vapor (Prospero and Nees, 1986; Prospero and Lamb 2003; Huang et al. 2009a-d). Some such factors can influence aerosol and precipitation simultaneously (for example Huang et al., 2009a-d for cases over tropical Atlantic); therefore, their effects should be addressed before examining the direct linkages between aerosol and precipitation.

2. Study Area and Methodology

The Seven SouthEast Asian Studies (7-SEAS, http://7-seas.gsfc.nasa.gov/) region covers a wide area from Java through the Malay Peninsula and Southeast Asia to Taiwan, where biomass burning smoke is the prevalent aerosol type. One of the seven scientific areas of interests of the 7-SEAS field campaign is to evaluate the impact of aerosol on cloud and precipitation. The region from the tropics to subtropics has significant gradients in air pollution varying from near pristine to heavily polluted atmospheric conditions. It therefore provides a unique natural laboratory for atmospheric measurements and aerosol-cloud-precipitation-climate interaction research. The cloud system in the region is so unique that they allow us to investigate not only the interactions of smoke and stratus clouds in the north but also the relations of smoke and deep convective cloud in the south.

In this paper, oriented by aerosol sources and cloud types, we will focus on two regions of interests (ROI) within the 7-SEAS region. The northern ROI (N-ROI) is from 5N to 30N, where biomass burning is active during early boreal spring, and smoke plumes are transported above low-level stratus over the South China Sea. An example from March 8, 2009 can be seen in Figure 1(a) where a heavy smoke layer was transported from biomass burning sources in Thailand to northern Vietnam, southern China and the South China Sea. Smoke layers appeared to be above the low-level stratus and significantly darkened the clouds. The southern ROI (S-ROI) is centered over Borneo and has a peak in aerosol loading in boreal fall. Figure 1(b) shows biomass burning over southern Borneo on October 5th 2006. The smoke was then transported westward and mixed with deep convective clouds over the Indian Ocean. Anthropogenic fires in equatorial Asia are one of the major contributors to global fire aerosol emissions along with Africa and South America (van der Werf et al., 2006, 2010). One focus of the upcoming SouthEast Asia Composition, Cloud, Climate Coupling Regional Study (SEAC4RS) campaign during August and September 2012 is on fire activity over equatorial Asia. The differences and similarities between the two ROI in the large-scale aerosol-precipitation covariability are of great interest to explore.

The main objective of this study is to explore the significance of the large-scale covariability between aerosol and precipitation in the 7-SEAS region from observational evidence perspective. The analysis was carried out in the following steps. Step 1: we first examine the large-scale covariability between aerosol and precipitation from long-term satellite datasets. ENSO effects are illustrated and removed. The response of rain characteristics to aerosols is also investigated. Step 2: to minimize the washout effect, we use carbon monoxide (CO) as a proxy for aerosol to reexamine the large-scale covariability between CO and precipitation in the same region. Step 3: to compare observational evidence to model simulations, we apply the similar data analysis approach to model simulations with both aerosol radiative and microphysical effects. Similarities and discrepancies from observations and simulations are compared. Step 4: To illustrate aerosol effects on clouds, we further investigate changes in cloud top height and outgoing longwave radiation in response to high aerosol scenarios. Step 5: We further explore the corresponding changes in the top of atmosphere (TOA) shortwave radiation flux to different aerosol anomalies. Step 6: The major ambient factor that influences aerosol effect on precipitation is liquid water path. We therefore further stratify liquid water path to reexamine aerosol-precipitation covariability. Step 7: we will repeat the data analysis in Step 1, 4 and 5 by using datasets from aerosol prevalent seasons only, to further evidence the seasonal significance of aerosol-precipitation covariability. The outcomes from the above analysis would help us to improve our current understanding of the aerosol-cloud-precipitation-climate interaction in this region.

Section 3 describes all the datasets we used in this study, followed by Section 4, which introduces all the findings. Section 5 concludes the study with summaries and discussions.

3. Datasets and Data Analysis

The major datasets used in this study are tabulated in Table 1. In Step 1 analysis, for aerosol, we used the Sea-viewing Wide Field-of-view Sensor (SeaWiFS) version 3 aerosol optical thickness (AOT, http://disc.sci.gsfc.nasa.gov/dust/; Sayer et al., 2011) as primary dataset, complemented by the Moderate Resolution Imaging Spectrometer (MODIS) AOT (Kaufman et al., 1997; Remer et al., 2005; Hsu et al. 2004, 2006) and the Total Ozone Mapping Spectrometer (TOMS) aerosol index (AI, Herman et al., 1997; Hsu et al., 1999). SeaWiFS AOT was preferred because of it is the longest single-sensor AOT dataset with retrievals over all surface land and ocean. For clouds, we used the International Satellite Cloud Climatology Project (ISCCP) cloud products for cloud type and cloud amount analysis (Schiffer et al., 1983). For precipitation, the Global Precipitation and Climatology Project (GPCP) (Huffman et al., 1997) and the Tropical Rainfall Measuring Mission (TRMM) precipitation products (Fisher, 2004) were used. TRMM was more preferable to match up with concurrent SeaWiFS aerosol retrievals owing to its higher temporal and spatial resolution. For Step 2 analysis, the AIRS carbon monoxide (CO) data (McMillan et al., 2011) were used as proxy of aerosol loading because CO is a direct product from biomass burning, and it is not washed out from the atmosphere by rain as easily as aerosols. For Step 3 analysis, a 5-year NCAR Community Atmosphere Model (CAM5) simulation, that includes both aerosol radiative and microphysical effects, were used to compare to observational evidence. For Step 4 analysis, the MODIS cloud top pressure (CTP, Menzel et al., 2008) and the NCEP-DOE Reanalysis II outgoing longwave radiation (OLR) data (Kanamitsu et al., 2002) were used to illustrate possible aerosol-cloud interaction mechanisms. For Step 5 analysis, the Cloud and Earth's Radiant Energy System (CERES) top of atmosphere (TOA) shortwave flux data at both clear sky and all-sky conditions (Wielicki et al, 1996) are used to observe the aerosol-related radiation changes. For Step 6, precipitation changes at different stratified liquid water paths retrieved from NCEP-DOE reanalysis II will be investigated to elucidate effects from ambient moisture. Lastly for Step 7, investigations are repeated using the above-mentioned datasets but for aerosol prevalent seasons only to further verify the significance of aerosol-induced cloud, precipitation and radiation changes in high aerosol scenarios.

Monthly datasets for aerosol, cloud, precipitation and radiation were used throughout the study, except the TRMM 3B42 daily rainfall data was used to count the number of days without rain ('no-rain days'). Monthly data was used because aerosol events in this region are usually of synoptic scale and therefore the aggregation from daily to monthly minimizes the impact of washout effect and cloud contamination on spatial completeness. Thus the relative comparison between monthly aerosol anomalies is not impacted by these effects as significantly as the relative comparison between daily aerosol anomalies. Raw data were detrended to remove long term trends. This is to avoid complications from variability at climate scale. Seasonal cycles were then removed so that we keep our primary focus on the anomalous changes of these parameters. Linear effects from ENSO were removed from the anomalies through a linear regression to calculate residual anomalies. Normalization was performed by dividing the residual anomalies by the corresponding seasonal cycle of standard deviation calculated from the raw data. In this way, the residual normalized anomalies are fairly comparable from month to month for evaluating effects from anomalous aerosol conditions on anomalous cloud and precipitation changes. To category high and low aerosol scenarios, the aerosol residual normalized anomalies are sorted into three (low, middle, and high) terciles. The corresponding residual anomalies of cloud and precipitation variables between high and low aerosol tercile months are compared and difference calculated to illustrate aerosol-associated variability.

4. Results

4.1 Aerosol, precipitation and cloud climatology

Figure 2 provides more information about the spatial variability of aerosol and precipitation during the two smoke-laden aerosol seasons: Feb-March-April for the North ROI (N-ROI) and Sep-Oct-Nov for the South ROI (S-ROI).

The N-ROI and S-ROI are shown in Figure 2(a) by dashed and solid outlines respectively. The aerosol domains (N-ROI, [10-30N, 95-130E]; S-ROI, [10S-10N, 95-130E]) are shown in yellow while the precipitation domains (N-ROI, [15-25N, 100-125E]; S-ROI, [5S-5N, 100-125E]) are shown in red. We selected a larger aerosol domain than precipitation domain to further overcome the potential complications from cloud contamination on aerosol data uncertainties. The assumption is that aerosol levels within clouds can be approximated by aerosol levels in closeby cloud-free retrievals because aerosol events are usually of synoptic scales therefore aerosol levels in the immediate adjacent cloud free vicinity are fairly similar to aerosol levels within the cloudy areas.

TOMS AI, with its capability to detect aerosol above clouds qualitatively, observed significant amount of aerosol in the N-ROI domain in early spring (Figure 2a). Similarly SeaWiFS AOT and MODIS AOT also showed a similar spatial pattern of aerosol in the same season. Such similarity in aerosol spatial distribution between AOT and AI in monthly data further evidences that 1) cloud contamination in monthly data is minimized in the daily-to-monthly data aggregation process, and 2) in monthly data, AOT is as indicative as AI to observe aerosol existence, despite the persistence of clouds in this region.

AIRS CO data also shows elevated level of CO over Thailand and the South China Sea in early spring and over Indonesia during fall, owing to biomass burning and atmospheric transport. However the spatial pattern of AOT and CO are not always consistent particularly during early spring when the CO distribution seems much stronger over South China Sea than over Northern Vietnam and Southern China, while AOT indicates the opposite patterns. Over S-ROI, on the other hand the spatial patterns of CO and AOT are more consistent with each other. Additionally, the overall enhanced signal in the AIRS CO data show a more widespread pattern of biomass burning emissions from the Borneo over the surrounding ocean regions, during autumn season relative to lower emissions during spring-time. The overall distribution for the two seasons suggests a shift of the enhanced biomass burning zone from the Indochina peninsula (during spring) to the equatorial islands (during autumn).

From precipitation data over the N-ROI during the premonsoon season in early spring, the stratus clouds that are often under the influence of smoke transported from the Indochina region do not precipitate much (monthly precipitation over N-ROI is less than 3 mm/day, Figure 2i). The deep convective rain in the South ROI, however, can produce 10 mm/day in both seasons (Figure 2i and 2j). It is worth pointing out that the regions are under the influence of different regimes such that the smoke aerosol prevails in a low precipitation efficiency stratus frontal system over the N-ROI, whereas the presence of smoke in the S-ROI co-exists in the deep convective cloud regime i.e., associated with higher precipitation efficiency.

The seasonal variation of aerosol and precipitation can also be seen in the time series in Figure 3. In general, both aerosol loading peaks in early spring and autumn during smoke seasons were well captured by TOMS AI, Aqua MODIS and SeaWiFS AOT, and AIRS CO measurements. Aqua MODIS and SeaWiFS AOT showed very comparable regional averaged AOT levels to each other while SeaWiFS has extended data record back to late 1997. It is also noteworthy that generally the AOT/AI peaks over the N-ROI are consistently higher than that over S-ROI from all three disparate satellite measurements (TOMS, SeaWiFS and MODIS). In addition, the CO time series also indicates a similar inter-annual variation with higher emissions over the N-ROI compared to S-ROI. Precipitation in N-ROI showed strong contrast between the boreal summer monsoon season and the rest of the seasons. In S-ROI, however, the seasonal contrast is not as significant as in N-ROI and the peak season is in boreal winter.

The fractional contributions from high, middle and low clouds as derived from ISCCP datasets over the two ROIs are shown in Figure 4. High and middle clouds that are strongly associated with deep convection are more often observed in S-ROI than in N-ROI (Figure 4a,b). In the contrast, low clouds that are usually stratus clouds in the 7-SEAS region are more prevalent in N-ROI (~25%) than in S-ROI (~15%) (Figure 4c). These observations of contrasting high and low cloud prevalence over the two regions are consistent within the general precipitation regimes of the 7-SEAS region.

4.2 Large-scale aerosol and precipitation covariability from satellite observations

Before the direct linkage between aerosol and precipitation are further investigated, it is crucial to minimize climate factor effects, such as ENSO, as these impact both aerosol and precipitation simultaneously. Relation between ENSO Nino3 index and precipitation anomalies is significantly negative at 95% confidence level over S-ROI but positive over N-ROI, as suggested by the spatial correlation distribution (Figure 5(a)). In contrast, ENSO Nino3 index and aerosol anomalies are positively correlated with 95% confidence level over S-ROI, suggesting the association of enhanced biomass burning activities with stronger ENSO signals, and a rather weak relationship is found over the N-ROI with a negative correlation at a less confidence level (Figure 5(b); Field et al., 2009). This implies that ENSO, as a climate factor, modulates aerosol and precipitation simultaneously. Over the 7-SEAS region, ENSO partially contributes to a negative large-scale covariability between aerosol and precipitation. In this study, ENSO effects on aerosol and precipitation were linearly removed through multivariate regression to focus on the aerosol-precipitation interactions that are independent of the modulating climate factors.

In the Step 1 analysis, we first calculated changes in the precipitation anomalies between high and low aerosol tercile months sorted by the normalized aerosol anomalies in order to identify covariability of aerosol and precipitation fields . Two independent runs were conducted for comparison: 1) SeaWiFS AOT vs. TRMM precipitation, for relatively short-term but high quality observational data (1998-2009 with two missing months, total 142 months); 2) TOMS AI vs. GPCP precipitation, for long-term datasets (1979-2000 with some data gaps, total 235 months). AOT difference between high and low aerosol tercile months were first shown in Figure 6(a) for N-ROI and 6(b) for S-ROI with a regional averages of 0.13 and 0.09 respectively. The large-scale covariability between aerosol and precipitation are more negative in the S-ROI shown in both long and short-term data analysis (Figure 6d vs. 6f). But the results from short-term and long-term data analysis are not so consistent for the N-ROI cases: it appears to be precipitation reduction in the TOMS AI vs. GPCP runs but precipitation increases in the SeaWiFS AOT vs. TRMM runs (Figure 6c vs. 6e). The low covariability between aerosol loading and precipitation over the N-ROI could be attributed to the low precipitation efficiency of the stratus clouds during pre-monsoon season.

Because the SeaWiFS data has similar overlapping coverage as TRMM, i.e. from 1997 onwards, and TRMM provides large variety of precipitation measurements, we were able to examine changes in rain rate and latent heating from TRMM TMI profiling product (3A12), no-rain days counted from TRMM daily precipitation product (3B42). Over the S-ROI, along with the reduction in total precipitation, rain intensity in terms of instantaneous rain rate increased while the number of raining days decreased between high and low aerosol terciles (Figure 7b and 7d). Systematic decreases of latent heating were observed below 10 km during anomalously high aerosol lading periods (Figure 7e and 7f), consistently indicating overall precipitation reduction at these levels. Over the N-ROI, however, the observed changes in rain rate, no-rain days and latent heating profiles were not as significant as over the S-ROI (Figure 7a,c and e). This is because stratus clouds over N-ROI are not usually precipitating. It is therefore difficult to measure marginal changes in precipitation attributable to changes in aerosol. On the other hand, deep convective clouds and precipitation are present in S-ROI most of the year. It was reported that aerosols induce cloud and precipitation suppression (Rosenfeld 1999) as well as invigoration (Koren et al., 2005; Rosenfeld et al., 2008) depending on ambient moisture conditions and sensitivity of cloud condensation nuclei (CCN) changes to aerosols. To further elucidate the mechanisms behind the negative large-scale covariability of aerosol and precipitation over the S-ROI, more observational and simulated evidences in Steps 2 to 7 is needed.

4.3 Large-scale CO and precipitation covariability

One of the largest complications to studying aerosol-precipitation interaction in the large-scale aerosol and precipitation covariability is the washout effect. Washout effect contributes to a negative relationship between aerosol loading and precipitation. As previously shown in Figure 2(d), (h) and Figure 3(a), CO, as produced from biomass burning, appears to resemble the aerosol variability pattern fairly well. However, as an atmospheric trace gas species, CO is not washed out by precipitation as effectively as aerosols are. Thus using CO as a proxy to approximate aerosols that modulate cloud and precipitation processes helps minimize the washout effect to some extent in the aerosol-precipitation studies.

Therefore in the Step 2 analysis, following the same data analysis procedure as in Step 1, large-scale covariability between CO and precipitation over N-ROI and S-ROI are shown in Figure 8. Over the S-ROI, higher CO concentration in the air is shown to be associated with significant precipitation reductions, while it is not significant in the N-ROI. These observations involving co-variability of CO and precipitation are similar to that previously shown using aerosol loading and precipitation. The implication is that, with less influence from wet removal, the aerosol-induced precipitation changes that are more attributable to aerosol radiative and microphysical effects, are more observable in the deep convective clouds than over the stratus with less precipitation. Over the equatorial Asia, the net aerosol radiative and microphysical effects are more likely to induce precipitation reduction.

4.4 Large-scale aerosol and precipitation covariability from model simulations

While observational evidence provides valuable inputs for model parameterization improvement, model simulation in turn helps identify aerosol effects from the observed aerosol and precipitation covariability. This requires comparisons between observational evidence and model simulations.

In the Step 3 analysis, 60-month CAM5 model simulations, which include both aerosol radiative and microphysical effects (Liu et al., 2011; Ghan et al., 2011), were used for this research. The large-scale covariability between model-simulated aerosol and precipitation was negative over S-ROI, in agreement with the results from observational evidences in Figure 6 (b, d) and 8(b). Over N-ROI however, precipitation changes between high and low aerosol terciles were less organized, similar to Figure 6(a) and 8(a). Therefore, model simulations of reduced precipitation over the equatorial Asia region support the observed covariability. From the point of view of model development, it is encouraging that the simulations matched observational patterns reasonably well. It is noteworthy however that the 60-month simulation is too short to draw any conclusive remarks. Longer model runs with only aerosol radiative forcing or only aerosol microphysical effect should be conducted in comparison to a reference run with only washout effect. In doing so, relative contributions from aerosol radiative and microphysical effects can thus be quantified with more confidence. Further investigations on those perspectives will follow this study.

4.5 Aerosols versus CTP and OLR

As discussed in the introduction, because of the coherent relationship between cloud and precipitation, thus aerosol-related cloud changes would subsequently induce precipitation changes. Therefore it is also of great interest to see how aerosols may impact cloud through aerosol-cloud interactions. In the Step 4 analysis of this study we explored the changes in cloud top pressure (CTP), cloud amount (CA) and outgoing longwave radiation (OLR) associated with aerosol loading anomalies, i.e. from aerosol low tercile to high tercile months. Figure 10 shows that over both N-ROI and S-ROI, there were clear increases of CTP but small decrease of CA, indicating less cloudiness with lower cloud top height in response to high AOT anomalies that also leads to increases of OLR. Interestingly, N-ROI also showed significant aerosol-induced changes in clouds although its changes in precipitation were not systematically observed in previous steps. The observed increase of CTP over the N-ROI as induced by smoke aerosols above stratus is consistent with the results of Wilcox (2010) that South African smoke over South Atlantic marine stratus leads to cloud layer subsidence, attributed to solar absorption by smoke above marine stratocumulus clouds increasing the buoyancy of free-tropospheric air above the temperature inversion capping the boundary layer. The observed CTP increase over the S-ROI is also in line with Huang et al. (2010a-d) that African aerosols were associated with suppression of deep convective cloud and precipitation over Atlantic Marine ITCZ and West African Monsoon, indicating cloud responses to more aerosol radiative forcing or semi-direct effects that overturns aerosol microphysical effects when aerosol anomalies are high (> 0.25). This is because very thick aerosol layers would reduce surface latent and sensible heating, warm the mid-troposphere, stabilize the atmosphere, results in less convection and convective rainfall (Ramanathan et al., 2001; Koren et al., 2008; Rosenfeld et al., 2008; Huang et al., 2009).

4.6 Aerosols versus Shortwave Radiation Flux

In clear sky conditions, aerosol radiative forcing can change the top of atmosphere (TOA) shortwave radiation fluxes via aerosol absorption and scattering. In aerosol-laden clouds, aerosols can also alter cloud albedo or cloudiness and consequently influence TOA shortwave radiation flux indirectly. To elucidate such aerosol effects, the differences in all-sky and clear sky shortwave flux between high and low aerosol tercile months are plotted in Figure 11.

For clear sky cases, both N-ROI and S-ROI indicated that high aerosol leads to higher TOA shorwave flux, which implies stronger aerosol scattering in the heavy aerosol laden atmosphere. This aerosol feedback signal seems rather stronger over S-ROI than over N-ROI, probably because the S-ROI is mostly ocean with darker surface so the aerosol-induced TOA shortwave flux increase is relatively larger and more observable.

For all-sky cases, both N-ROI and S-ROI also consistently showed negative changes in the TOA shortwave flux. Over N-ROI, there are two reasons for explanation: Firstly, aerosols are frequently transported above stratus clouds, darken the clouds by reducing cloud albedo and thus reduce TOA shortwave flux. Secondly, aerosol reduces cloud top height as seen in the increased cloud top pressure in Figure 10. Consequently, such aerosol-induced changes in cloud optical properties also impact

TOA shortwave flux. For example, lower cloud optical depth would have less cloud scattering and thus result in decreased TOA shortwave flux. Over S-ROI however, aerosols are normally mixed with deep convective clouds. Aerosol can also change cloud albedo because aerosols increase number of cloud condensation nuclei (CCN) and result in more absorbing cloud particle (cloud albedo effect). Secondly, aerosol is also related to suppression deep convection, seen as the increased cloud top pressure and outgoing long wave radiation in Figure 10. Therefore the aerosol-induced negative changes of cloud scattering significantly decreases TOA shortwave radiation flux (Figure 11).

4.7 Stratifications of cloud liquid water path

One factor is the ambient moisture or water vapor that also modulates cloud formation and precipitation processes. To further elucidate our observed aerosol and precipitation covariability is not sensitive to water vapor in this region, in Step 5 of our analysis, we stratified concurrent liquid water path (LWP) into three terciles, and calculated precipitation changes between high and low aerosol tercile months same as in Figure 6 but under at high and low LWP terciles respectively.

Figure 12 compares the results from low and high LWP conditions over S-ROI only. In general, the large-scale negative covariability between aerosol and precipitation persisted under both low and high LWP conditions, which means water vapor effect alone cannot explain the covariability observed in Figures 6-9 and thus evident the observability of large-scale aerosol effects on precipitation. However the reduction in precipitation seems more significant in the high LWP conditions (Figure 12(b)).

Because LWP and precipitation anomalies are usually positively correlated, such enhancement of precipitation suppression owing to higher LWP condition actually indicates that if aerosol effects on deep convective precipitation are significant and observable from both observations and models as in Figure 6-10, it favors moist conditions more than dry conditions. Such LWP preference of precipitation suppression is consistent with Fan et al. (2009) for deep convective cases that the decreasing rate of convective strength is greater in humid air than that in dry air when wind shear is strong.

4.8 Precipitation-Cloud-Radiation Changes in Aerosol Prevalent Seasons

As discussed in the previous steps, aerosol effects on cloud, precipitation and radiation are seemingly significant. More convincing evidence should be seen in aerosol prevalent seasons when changes in aerosol anomalies are larger. Thus, we focus our analysis on boreal early spring season (Feb-Mar-Apr) for N-ROI case and boreal fall season (Sep-Oct-Nov) for S-ROI case and calculate the difference composites of precipitation, all-sky shortwave TOA flux, and cloud top pressure (Figure 13). In comparison to the figures with all season datasets (Figure 6 for precipitation, Figure 10 for CTP, Figure 11 for SW flux), the changes in all three parameters were much larger in comparison to the all season cases. In general, precipitation inhibition, cloud top suppression, and reduction of all-sky shortwave TOA flux were significantly observed in the aerosol prevalent seasons over both N-ROI and S-ROI. This further evidences the sensitivity of these meteorological parameters to aerosol changes because aerosol is a more predominant factor in the weather system during these aerosol prevalent seasons.

5. Summary and Discussions

We investigated the large-scale covariability between aerosol, cloud, precipitation, and radiation over the 7-SEAS region by using both satellite observations and model simulations. The study was conducted in seven major steps of analysis: 1) observational evidence of large-scale aerosol and precipitation covariability; 2) observational evidence of large-scale CO and precipitation covariability; 3) model simulations of large-scale aerosol and precipitation covariability; 4) observational evidence of large-scale aerosol and cloud covariability; 5) observational evidence of large-scale aerosol and shortwave radiation; 6) stratification of cloud liquid water path in the large-scale aerosol and precipitation covariability; 7) observational evidence in aerosol prevalent seasons.

Main results are summarized in Table 2:

Over the deep convective regime in the S-ROI, high aerosols loading is associated with overall reduced total precipitation (-1.23 mm/day and -1.53 mm/day from two independent analysis) with intensified rain rates (+0.029 mm/day) and decreased rain frequency (+4 no-rain days), decreased tropospheric latent heating, suppressed cloud top height (+26.8hPa in CTP) and cloud amount (-1.8%), increased outgoing longwave radiation (+4.41W/m^2), enhanced clear-sky shortwave TOA flux (+2.59W/m^2), but reduced all-sky shortwave TOA flux (-4.20W/m^2).

In contrast over the stratus cloud regime in the N-ROI, the overall changes in the cloud, precipitation, and radiation variables between high and low aerosol scenarios are less significant. In anomalously high aerosol loading scenario, precipitation changes are not consistent in two independent analysis (-0.30 mm/day vs. +0.31 mm/day) but rain rates decrease (-0.11 mm/day) with slight higher rain frequency (-1 no-rain days). High aerosol loadings are also associated with decreased tropospheric latent heating, slightly suppressed cloud top height (+4.36 hPa in CTP) and very marginal change of cloud amount (-0.12%), increased outgoing longwave radiation (+3.21 W/m^2), enhanced clear-sky shortwave TOA flux (+1.36 W/m^2), but reduced all-sky shortwave TOA flux (-0.41 W/m^2).

More detailed summary and discussions are organized in the following key points:

1) The 7-SEAS region provides us with a unique testbed for observing the climatic effects of biomass burning aerosols on cloud and precipitation due to its active biomass burning activities. Moreover, the different cloud systems in the Northern and Southern parts of the region allow us to directly compare different characteristics of large-scale aerosol and precipitation covariability in different cloud regimes. The upcoming SouthEast Asia Composition, Cloud, Climate Coupling Regional Study (SEAC4RS) campaign, with its focus of aerosol-cloud-precipitation interaction in tropical Asia in August and September 2012, will provide valuable in-situ radiometric measurements to further support or verify the satellite and model results we show in this

study. Furthermore, this study provides more valuable information on the regional scale covariability of aerosol-cloud-precipitation interactions.

2) Large-scale aerosol and precipitation covariability consists of three major components: aerosol effects on precipitation, washout effect, and climate factor effects. Observational evidence has to be investigated along with model simulations to truly separate the components explicitly. However, observational evidence can still provide useful insights to better understand the overall climatic effects of aerosol. For example, the consistency between aerosol-precipitation covariability and CO-precipitation covariability can help us better understand the significance of aerosol effects on precipitation, by minimizing the washout effect. In addition, ENSO can modulate aerosol and precipitation variability in this region simultaneously. Therefore it is important to separate the three components, with the assistance from observations and simulations, before any quantitative evaluation of global or regional scale aerosol climatic effects are conducted.

3) Large-scale covariability between aerosol and precipitation are different over the stratus region in N-ROI and the deep convective cloud region in S-ROI. From the sequential Step 1 to Step 5 analysis, both satellite observations and model simulations observed systematic negative covariability between aerosol and precipitation. Although eventually we have to rely on model simulations to demonstrate the exact dominant aerosol effect in this region, it is encouraging that the large-scale aerosol and precipitation covariability from observations and model simulations bear some notable similarities. We now know that a negative aerosol-precipitation interaction more likely occurs in the deep convective cloud system in the 7-SEAS region. More model runs are needed to further pinpoint different aerosol effects on precipitation and quantify their

relative contributions. Over the N-ROI however, although aerosol-stratus interaction can still be active, due to the generally non-precipitating nature of stratus clouds, it is harder to observe aerosol-precipitation covariability there. However it is noteworthy that although precipitation change is less certain, the aerosol associated cloud and radiation changes are as significant over the N-ROI as over the S-ROI.

4) There remain uncertain factors that can influence the aerosol-precipitation interactions. For example, although the negative aerosol and precipitation covariability were observed for both high and low cloud liquid water path conditions, moist conditions seem to enhance the precipitation reductions that are attributable to aerosol increases. Moreover, in the vicinity of the western tropical Pacific, the large-scale dynamics over the 7-SEAS region is very strong. It is still unknown but intriguing that how the large-scale aerosol and precipitation covariability would be at different Madden-Julian Oscillation (MJO) phases, a dominant rainfall feature in this region. Moreover, because aerosol emissions usually occur in the pre-monsoon seasons in this area, it is also worthwhile exploring whether anomalous aerosol loadings would impact large-scale dynamic fields through its radiative forcing and, subsequently, affect monsoon rainfall. For example, does the aerosol elevated heat pump (EHP) effect significantly impact precipitation in this region?

5) For deep convective clouds in the S-ROI, theoretically, aerosol microphysical effects lead to smaller cloud particle sizes, delay warm rain precipitation processes and invigorate deep convection (Koren et al., 2005; Rosenfeld et al., 2008). The aerosol semi-direct effect on other hand can reduce cloud by increasing tropospheric heating in the clouds. Aerosol radiative forcing also suppresses convective clouds by the increased environmental stability in respond to aerosol absorption (Cook and Highwood, 2003).

Rosenfeld et al. (2008) suggest an aerosol concentration saturation point at which the fractional contributions from aerosol radiative and microphysical effects will vary to limit convective potential. From the shown evidence in this study, the net aerosol effect on precipitation and cloud deep convection is more negative, in line with aerosol radiative forcing described above but not the invigoration of deep convection as suggested by aerosol microphysical effect described in Rosenfeld et al. (2008) and model simulations from Lebo and Seinfeld (2011). More climate model runs with different aerosol effect in place will help to elucidate the mechanisms better.

6) Data uncertainty could still be a significant issue for this study or similar ones, particularly aerosol observations. It is still challenging for us to completely understand the complicated climate systems over this region, particularly when cloud coverage is so prevalent to prevent extensive aerosol observations. It is not yet possible for satellites to retrieve aerosol optical properties within or beneath clouds yet, although the UV based aerosol index is able to detect aerosol qualitatively above clouds. In this study we used statistical techniques to minimize data uncertainties, for example, using monthly data other than daily data and selecting larger aerosol domain than precipitation domain. However, we cannot completely rule out data uncertainty issues to make the results more conclusive. For example, the discrepancy between the TOMS AI vs. GPCP run and the SeaWiFS AOT vs. TRMM run (Figure 6c vs. Figure 6e) could be partially because that TOMS AI can observe aerosols above clouds but SeaWiFS AOT cannot.

Overall, the study provides us a big picture of the characterizations of the large-scale covariability between aerosol, cloud and precipitation over the 7-SEAS region. More systematic investigations will continue to explore more fundamental mechanisms that are modulating the weather and climate systems in the region.

Acknowledgement

This work is supported by grant from the NASA EOS Program, managed by Hal Maring. The authors acknowledge NCDC of NOAA (http://lwf.ncdc.noaa.gov/oa/wmo/wdcamet-ncdc.html) for data provision of GPCP version 2 data and NCEP-DOE reanalysis II data, NASA GSFC (http://toms.gsfc.nasa.gov/aerosols/aerosols_v8.html) for data provision of TOMS AI, and the Data and Information Services Center (DISC) of NASA (http://disc.sci.gsfc.nasa.gov/) for data provision of TRMM, AIRS, MODIS and SeaWiFS data. The Pacific Northwest National Laboratory (PNNL) is operated for the DOE by Battelle Memorial Institute under contract DE-AC06-76RLO 1830.

References

Ackerman, A. S., O. B. Toon, D. E. Stevens, A. J. Heymsfield, V. Ramanathan and E. J. Welton, 2000: Reduction of Tropical Cloudiness by Soot. Science, 288(5), 1042-1047.

Albrecht, B., 1989: Aerosols, cloud microphysics, and fractional cloudiness. Science, 245, 1227–1230.

Carlson, T. N., and S. G. Benjamin, 1980: Radiative heating rates for Saharan dust. J. Atmos. Sci., 37, 193–213.

Cook, J. and E. J. Highwood, 2003: Climate response to tropospheric absorbing aerosols in an Intermediate General-Circulation Model. Q. J. R. Meteorol. Soc., 1, 1-20.

Diaz, J. P., F. J. Exposito, C. J. Torres, F. Herrera, J. M. Prospero, and M. C. Romero, 2001: Radiative properties of aerosols in Saharan dust outbreaks using ground-based and satellite data: Applications to radiative forcing. J. Geophys. Res., 106, 18403–18416.

Fan, J., T. Yuan, J. M. Comstock, S. Ghan, A. Khain, L. R. Leung, Z. Li, V. J. Martins, and M. Ovchinnikov (2009), Dominant role by vertical wind shear in regulating aerosol effects on deep convective clouds, J. Geophys. Res., 114, D22206, doi:10.1029/2009JD012352.

Feingold, G., L. A. Remer, J. Ramaprasad and Y. J. Kaufman, 2001: Analysis of smoke impact on clouds in Brazilian biomass burning regions: An extension of Twomey's approach. J. Geophys. Res., 106(D19), 22907-22922.

Field, R. D., G. R. van der Werf and S. S. P. Shen, 2009: Human amplification of drought induced biomass burning in Indonesia since 1960. Nature Geo., 2, 185-188.

Fisher L. B., 2004: Climatological validation of TRMM TMI and PR monthly rain products over Oklahoma J. Appl. Meteorol. 43, 519–35.

Ghan, S. J., **X. Liu**, R. C. Easter, P. Rasch, J.-H. Yoon, Toward a Minimal Representation of Aerosol Direct, Semi-Direct and Indirect Effects: Comparative Decomposition, *Journal of Climate*, submitted, 2011.

Hao, W. M., and M. Liu, 1994: Spatial and temporal distribution of tropical biomass burning. Global Biogeochem. Cycles, 8, 495–504.

Herman, J. R., P. K. Bhartia, O. Torres, C. Hsu, C. Seftor, and E. Celarier (1997), Global distribution of UV-absorbing aerosols from Nimbus 7/TOMS data, J. Geophys. Res., 102(D14), 16,911–16,922, doi:10.1029/96JD03680.

Hsu N.C., J.R. Herman, O. Torres, B. N. Holben, Tanre, and T. F. Eck (1999). Comparisons of the TOMS aerosol index and the sun photometer aerosol optical thickness: Results and applications, J. Geophys. Res., 6269-6279, 104

Hsu, N.C.; Si-Chee Tsay; King, M.D.; Herman, J.R., 2004: Aerosol properties over bright-reflecting source regions," Geoscience and Remote Sensing, IEEE Transactions on , vol.42, no.3, pp. 557- 569, March 2004, doi: 10.1109/TGRS.2004.824067

Hsu, N. C., S. C. Tsay, M. D. King, and J. R. Herman, 2006: Deep blue retrievals of Asian aerosol properties during ACE-Asia. IEEE Trans. Geosci. Remote Sens., 44, 3180-3195.

Huang, J., C. Zhang, J. M. Prospero., 2009a: Aerosol-induced large-scale variability in precipitation over the tropical Atlantic. J. Climate, 22, 4970–4988. doi: 10.1175/2009JCLI2531.1

Huang, J., C. Zhang, J. M. Prospero, 2009b: Large-scale effect of aerosols on precipitation in the West African Monsoon region. Quarterly Journal of the Royal Meteorological Society 135:640, 581-594.

Huang, J., Zhang, C., Prospero, J. M., 2009c, Large-scale variability of aerosol and precipitation in the West African Monsoon, Environmental Research Letter, 4, 015006, doi:10.1088/1748-9326/4/1/015006, 2009

Huang, J., A. Adams, C. Wang, and C. Zhang, 2009d, Black Carbon and West African Monsoon precipitation: observations and simulations, Annales Geophysicae, Special Issue: From Deserts to Monsoons – First International Aegean Workshop, 27, 4171-4181, 2009

Huffman, G. J., and Coauthors, 1997: The Global Precipitation Climatology Project (GPCP) Combined Precipitation Data Set. Bull. Amer. Meteor. Soc., 78, 5–20.

Intergovernmental Panel on Climate Change (IPCC), Climate Change 2007: The Physical Sciences Basis, Cambridge University Press, New York, 2007.

Kanamitsu,M., W. Ebisuzaki, J. Woollen, S-K Yang, J.J. Hnilo, M. Fiorino, and G. L. Potter.,NCEP-DEO AMIP-II Reanalysis (R-2), 1631-1643, Nov 2002, Bul. of the Atmos. Met. Soc.

Kaufman, Y. J., Tanre, D., Remer, L., Vermote, E., Chu, A., and Holben, B. N.: Operational remote sensing of tropospheric aerosol over land from EOS moderate resolution imaging spectroradiometer, J. Geophys. Res.-Atmos., 102(D14), 17051–17067, 1997.

Khain, A. P., N. BenMoshe, A. Pokrovsky, 2008: Factors Determining the Impact of Aerosols on Surface Precipitation from Clouds: An Attempt at Classification. *J. Atmos. Sci.*, **65**, 1721–1748. doi: 10.1175/2007JAS2515.1

Koren, I., Y. J. Kaufman, L. A. Remer and J. V. Martins, 2004: Measurement of the Effect of Amazon Smoke on Inhibition of Cloud Formation. Science, 303, 1342-1345.

Koren, I., Y. J. Kaufman, D. Rosenfeld, L. A. Remer and Y. Rudich, 2005: Aerosol invigoration and restructuring of Atlantic clouds. Geophys. Res. Lett., 32, L14828.

Koren, I., J. V. Martins, L. A. Remer, and H. Afargan (2008), Smoke invigoration versus inhibition of clouds over the Amazon, Science, 321, 946–949, doi:10.1126/science.1159185.

Lau, K.M., M. K. Kim, and K.M. Kim (2006), Aerosol induced anomalies in the Asian summer monsoon the role of the Tibetan Plateau, Clim. Dyn., 26, 855–864, doi:10.1007/s00382-006-0114-z.

Lebo, Z. J. and Seinfeld, J. H.: Theoretical basis for convective invigoration due to increased aerosol concentration, Atmos. Chem. Phys., 11, 5407-5429, doi:10.5194/acp-11-5407-2011, 2011.

Liu, X., R. C. Easter, S. J. Ghan, R. Zaveri, P. Rasch, X. Shi, J.-F. Lamarque, A. Gettelman, H. Morrison, F. Vitt, A. Conley, S. Park, R. Neale, C. Hannay, A. Ekman, P. Hess, N. Mahowald, W. Collins, M. Iacono, C. Bretherton, and M. Flanner, Toward a Minimal Representation of Aerosol Direct and Indirect Effects: Model Description and Evaluation. *Geoscientific Model Development Discussion, 4*, 3485-3598, doi:10.5194/gmdd-4-3485-2011, 2011.

Lohmann, U., and J. Feichter, 2005: Global indirect aerosol effects: a review. Atmos. Chem. Phys., 5, 715–737.

McMillan, W.W.; Evans, K.D.; Barnet, C.D.; Maddy, E.S.; Sachse, G.W.; Diskin, G.S.; , "Validating the AIRS Version 5 CO Retrieval With DACOM In Situ Measurements During INTEX-A and -B," Geoscience and Remote Sensing, IEEE Transactions on , vol.49, no.7, pp.2802-2813, July 2011, doi: 10.1109/TGRS.2011.2106505

Menzel, W. Paul, R. A. Frey, H. Zhang, D. P. Wylie, C. C. Moeller, R. E. Holz, B. Maddux, B. A. Baum, K.I. Strabala, and L. E. Gumley, 2008: MODIS Global Cloud-Top Pressure and Amount Estimation: Algorithm Description and Results. *J. Appl. Meteor. Climatol.*, **47**, 1175–1198.doi: http://dx.doi.org/10.1175/2007JAMC1705.1

Miller, R. L., and I. Tegen, 1998: Climate response to soil dust aerosols. J. Climate, 11, 3247–3267.

Prospero, J. M., and J. P. Lamb, 2003: African droughts and dust transport to the Caribbean: Climate change and implications. *Science*, **302,** 1024–1027.

Prospero, J. M., and R. T. Nees, 1986: Impact of North African drought and El Niño on mineral dust in the Barbados trade winds. *Nature*, **320,** 735–738.

Ramanathan, V., P. J. Crutzen, J. T. Kiehl, and D. Rosenfeld, 2001: Aerosols, climate, and the hydrological cycle. Science, 294, 2119–2124.

Remer, L., Kaufman, Y., Tanre, D., Mattoo, S., Chu, D., Martins, J., et al.: The MODIS aerosol algorithm, products, and validation, J. Atmos. Sci., 62(4), 947–973, 2005.

Rosenfeld, D., 1999: TRMM observed first direct evidence of smoke from forest fires inhibiting rainfall. Geophys. Res. Lett., 26(20), 3105.

Rosenfeld, D., U. Lohmann, G. B. Raga, C. D. O'Dowd, M. Kulmala, S. Fuzzi, A. Reissell, and M. O. Andreae, Flood or Drought: How Do Aerosols Affect Precipitation?, 2008: Science, 321 (5894), 1309-1313. [DOI:10.1126/science.1160606]

Rotstayn, L. D., and Coauthors, 2007: Have Australian rainfall and cloudiness increased due to the remote effects of Asian anthropogenic aerosols? J. Geophys. Res., 112, D09202. doi:10.1029/2006JD007712.

Sassen, K., P. J. DeMott, J. M. Prospero, and M. R. Poellot, 2003: Saharan dust storms and indirect aerosol effects on clouds: CRYSTAL-FACE results. Geophys. Res. Lett., 30, 1633.

Sayer, A. M., N. C. Hsu, C. Bettenhausen, Z. Ahmad, B. Holben, A. Smirnov, G. E. Thomas , J. Zhang, SeaWiFS Ocean Aerosol Retrieval (SOAR): algorithm, validation, and comparison with other datasets, J. Geophys. Res., submitted, 2011

Schiffer, R.A., and W.B. Rossow, 1983: The International Satellite Cloud Climatology Project (ISCCP): The first project of the World Climate Research Programme. Bull. Amer. Meteorol. Soc., 64, 779-784.

Twomey, S. A., M. Piepgrass, and T. L. Wolfe, 1984: An assessment of the impact of pollution on the global albedo. Tellus, 36, 356–366.

van der Werf, G. R., J. T. Randerson, L. Giglio, G. T. Collat, P. S. Kasibhatla and A. S. Arellano Jr., 2006: Interannual variability in global biomass burning emissions from 1997 to 2004. Atmos. Chem. and Phys., 6(5), 3423-3441.

van derWerf, G. R., J. T. Randerson, L. Giglio, G. J. Collatz, M. Mu, P. S. Kasibhatla, D. C. Morton, R. S. DeFries, Y. Jin and T. T. van Leeuwen, 2010: Global fire emissions and the contribution of deforestation, savanna, forest, agricultural, and peat fires (1997-2009). Atmos. Chem. and Phys., **10**, 11707-117353423-3441.

Wielicki, B. A., B. R. Barkstrom, E. F. Harrison, R. B. Lee III, G. L. Smith, and J. E. Cooper, "Clouds and the Earth's Radiant Energy System (CERES): An Earth Observing System Experiment," Bull. Amer. Meteor. Soc., 77, 853-868, 1996.

Wilcox, E. M., Stratus cloud thickening beneath layers of absorbing smoke aerosol. Atmos. Chem. Phys., 10, 11769-11777,doi:10.5194/acp-10-11769-2010, 2010.

Yoshioka, M., N. Mahowald, A. Conley, W. Collins, D. Fillmore, C. Zender, and D.

Coleman, 2007: Impact of desert dust radiative forcing on Sahel precipitation: Relative importance of dust compared to sea surface temperature variations, vegetation changes, and greenhouse gas warming. J. Climate, 20, 1445–1467.

Table 1. The major satellite observed and model simulated datasets used in this study

Data Source	Parameter	Coverage	Length (months)	Unit
SeaWiFS	AOT	1997.09-2010.12, 2 missing months	158	Unitless
MODIS	AOT	2002.07-2010.04	94	Unitless
MODIS	CTP	2002.07-2010.04	94	hPa
TRMM 3B43	Monthly total rain	1998.01-2009.12	144	mm/day
TRMM 3B42	Daily total rain	1998.01-2009.12	144	mm/day
TRMM 3A12	Monthly rain rate	1998.01-2009.12	144	mm/day
TRMM 3A12	Monthly latent heating	1998.01-2009.12	144	K/hour
NOAA OI	SST	1981.12-2010.04	341	K
GPCP	Precipitation	1979.01-2009.09	369	mm/day
TOMS	AI	1978.11-1993.04; 1996.08-2000.12	237	Unitless
AIRS	CO	2002.09-2011.08	108	10^{18} molecular/cm^2
NCEP-DOE reanalysis II	OLR	1974.06-2010.04	431	W/m^2
NCEP-DOE reanalysis II	LWP	1979.01-2011.07	391	kg/m^2
ISCCP	Cloud Amount	1983.01-2007.12	300	Unitless
CAM5	AOT, Precipitation		60	AOT-Unitless Precipitation-mm/day
CERES	TOA SW Flux	2000.03-2010.12	130	W/m^2

Table 2. The domain-averaged changes in the anomalies of aerosol, cloud, precipitation, radiation variables between high and low tercile months of aerosol normalized anomalies. Negative changes are in **bold** and positive changes in *italic.*

	SeaWiFS AOT	GPCP Precip.	TRMM Precip.	TRMM Rain Rate	TRMM no-rain Days	MODIS CTP	NCEP OLR	CERES TOA SW Clear-Sky	CERES TOA SW All-Sky	ISCCP Cloud Amount
unit	unitless	mm/day	mm/day	mm/day	days	hPa	W/m^2	W/m^2	W/m^2	%
S-ROI	*+0.13*	**-1.23**	**-1.53**	*+0.029*	*+4*	*+26.8*	*+4.41*	*+2.59*	**-4.20**	**-1.80**
N-ROI	*+0.089*	**-0.30**	*+0.31*	**-0.11**	**-1**	*+4.36*	*+3.21*	*+1.36*	**-0.41**	**-0.12**

(a) RGB, 03/08/2009 (b) RGB, 10/05/2006

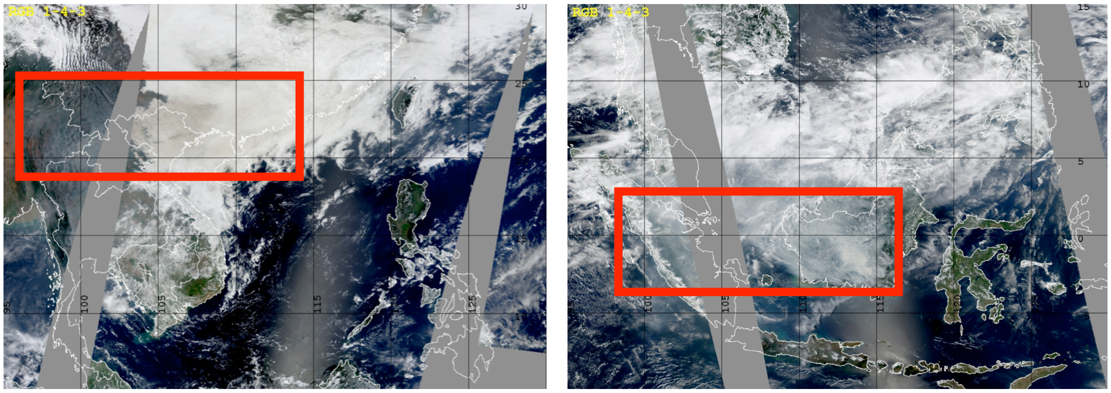

Figure 1. (a) Terra MODIS RGB Images over the Northern ROI on March 8, 2009, showing a smoke plume was transported by westerly jet from western source regions to above stratus clouds over Northern Vietnam and Northern South China Sea; (b) Aqua MODIS RGB image over the Southern ROI on October 5, 2006, showing biomass burning over Borneo island, Indonesia, and the smoke plume was transported by easterly jet from Borneo to Indian Ocean.

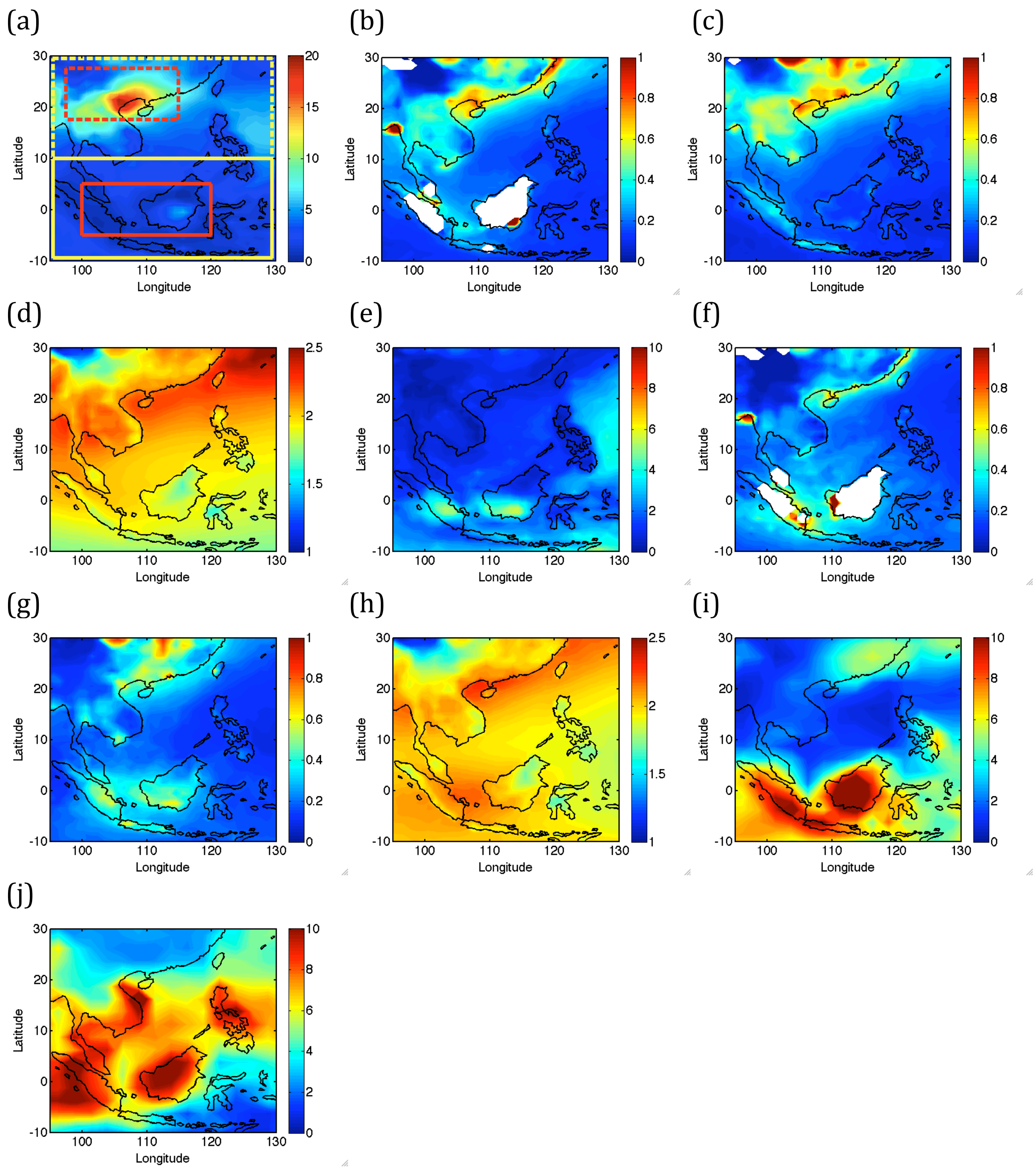

Figure 2. Spatial pattern of seasonal aerosol and precipitation. (a) to (d) are the Feb-Mar-Apr seasonal mean of (a) TOMS AI; (b) SeaWiFS AOT; (c) MODIS AOT; (d) AIRS CO (10^{18} molecular/cm^2). (e) to (h) are the Sep-Oct-Nov seasonal mean of (e) TOMS AI; (f) SeaWiFS AOT; (g) MODIS AOT; (h) AIRS CO. The corresponding seasonal GPCP precipitation are: (i) Feb-Mar-Apr; (j) Sep-Oct-Nov. The N-ROI and S-ROI were defined in Figure 2(a) where yellow outlines for aerosol domains and red outlines for precipitation domains for the N-ROI (in dashed lines) and the S-ROI (in solid lines) respectively.

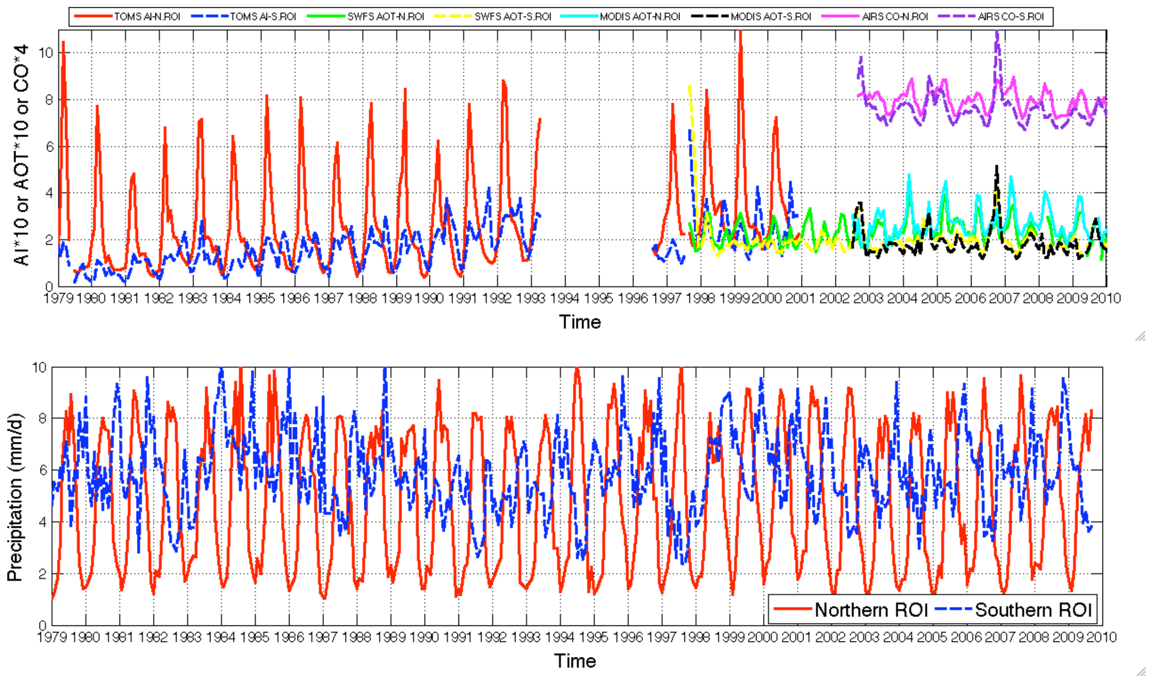

Figure 3. Time series of aerosol and precipitation over the Northern and Southern ROI. AI and AOT are unitless. CO has unit of 10^{18} molecular/cm^2. Precipitation has unit of mm/day.

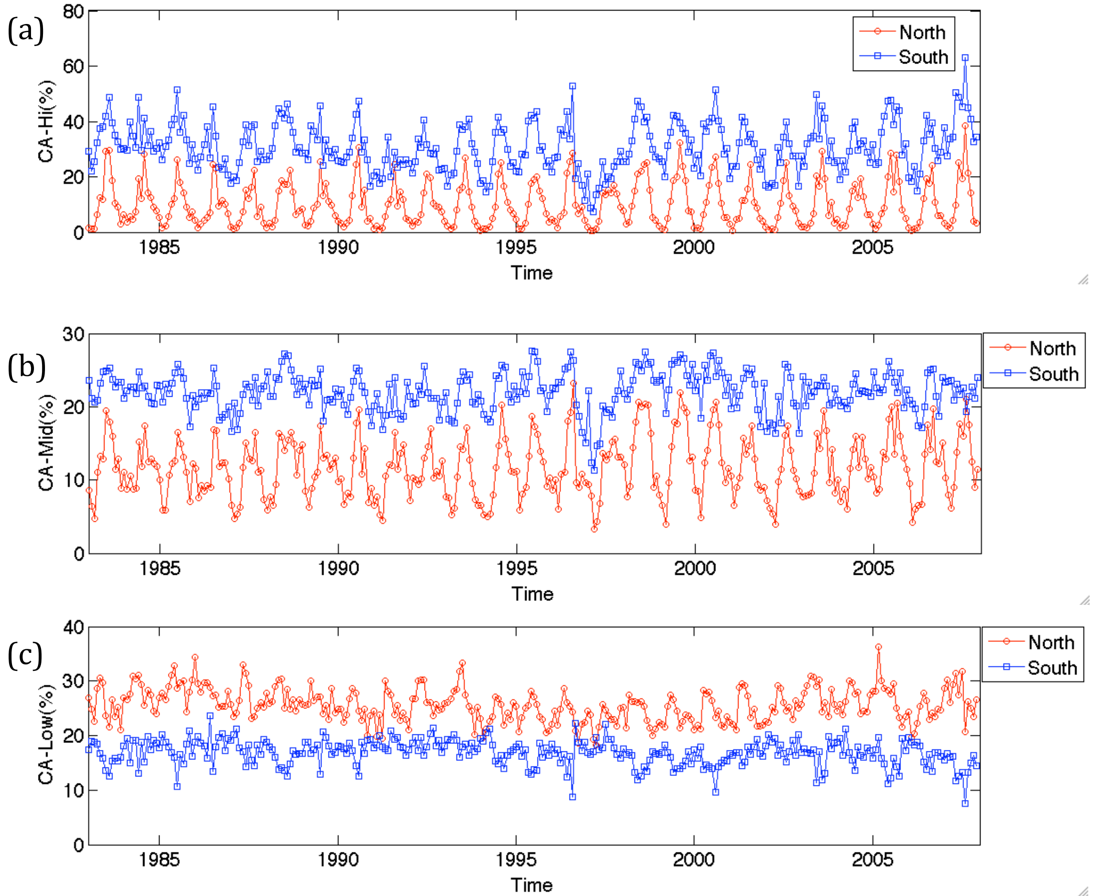

Figure 4. High, middle and low cloud amounts in the northern and southern ROIs: (a) high cloud; (b) middle cloud; (c) low cloud.

(a) Nino3 vs. Precipitation (b) Nino3 vs. Aerosol

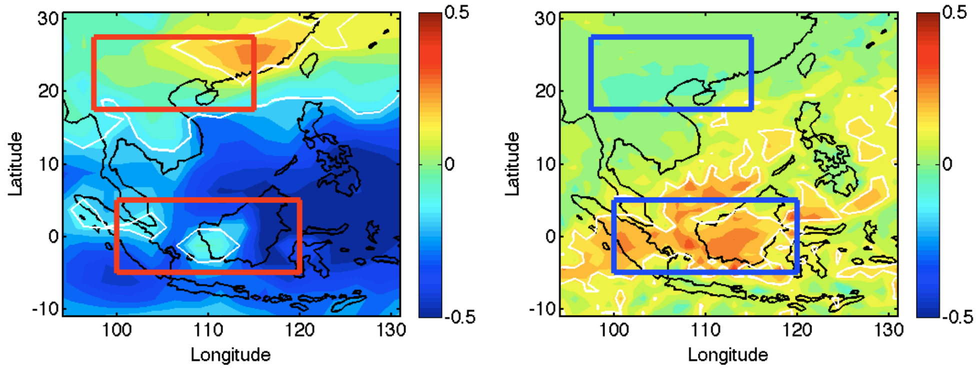

Figure 5. (a) Correlation between ENSO NINO3 index and GPCP precipitation anomalies; and (b) correlation between ENSO NINO3 index and TOMS AI anomalies. The white contours mark 95% confidence level on the correlation significance.

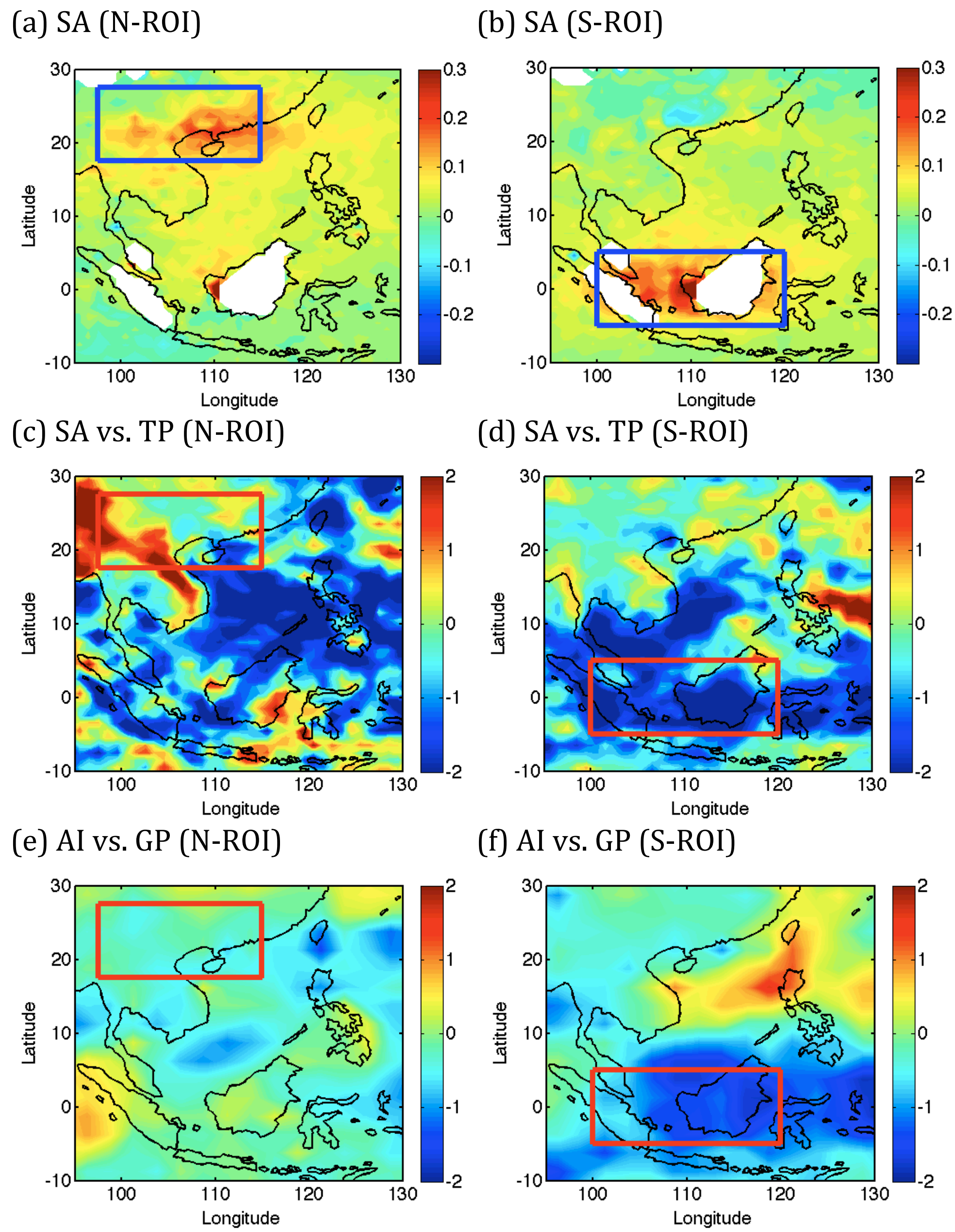

Figure 6. Differences in SeaWiFS aerosol anomalies between high and low aerosol tercile months: (a) for N-ROI, and (b) for S-ROI. And the corresponding changes in precipitation anomalies between high and low aerosol tercile months in aerosol normalized anomalies: (c) SeaWiFS AOT vs. TRMM precipitation at N-ROI; (d) SeaWiFS AOT vs. TRMM precipitation at S-ROI; (e) TOMS AI vs. GPCP precipitation at N-ROI; (f) TOMS AI vs. GPCP precipitation at S-ROI. (SA: SeaWiFS AOT; AI: TOMS Aerosol Index; TP: TRMM Precipitation; GP: GPCP precipitation). Square boxes were used to highlight the areas of interests.

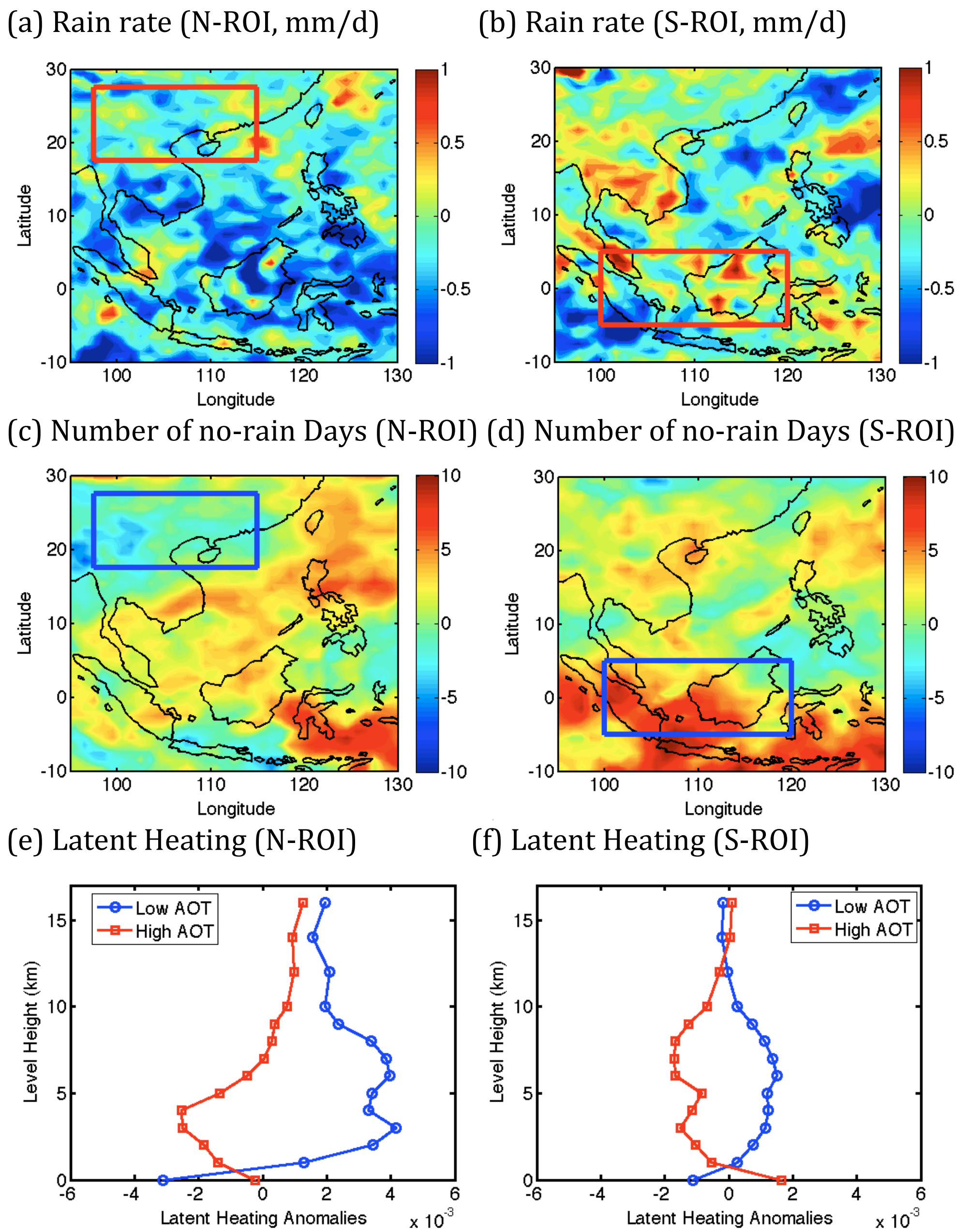

Figure 7. Difference composite of anomalies in (a, b) rain intensity, (c, d) no-rain days and (e, f) latent heating profiles between high and low terciles of normalized aerosol anomalies, for N-ROI (left) and S-ROI (right) respectively.

(a) CO vs. Total Rain (N-ROI) (b) CO vs. Total Rain (S-ROI)

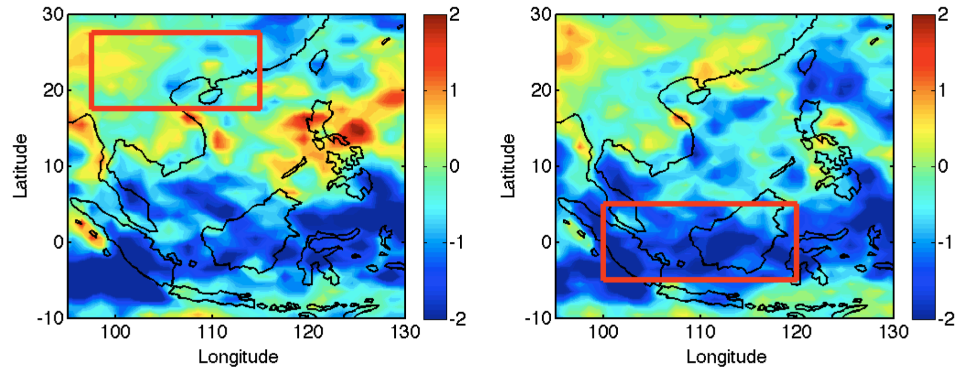

Figure 8. Difference composites of total rain anomalies between high and low tercile months of CO normalized anomalies

(a) AOT vs. Total Rain (N-ROI) (b) AOT vs. Total Rain (S-ROI)

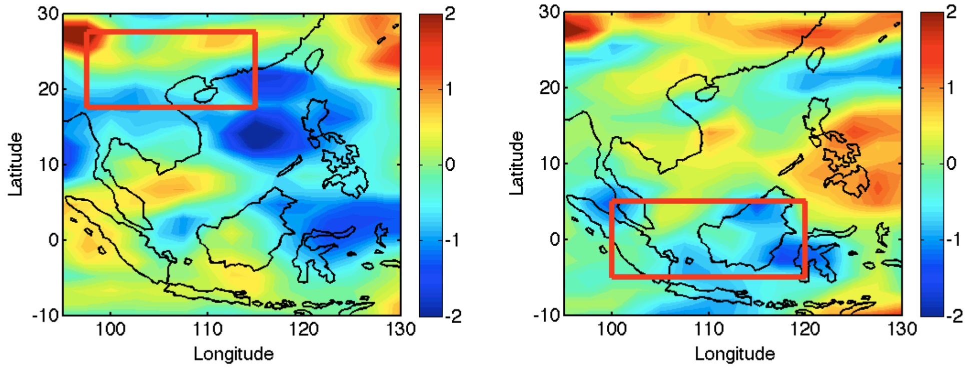

Figure 9. Model simulations from CAM5: Difference composites of total rain anomalies between high and low tercile months of aerosol normalized anomalies (a) N-ROI; (b) S-ROI.

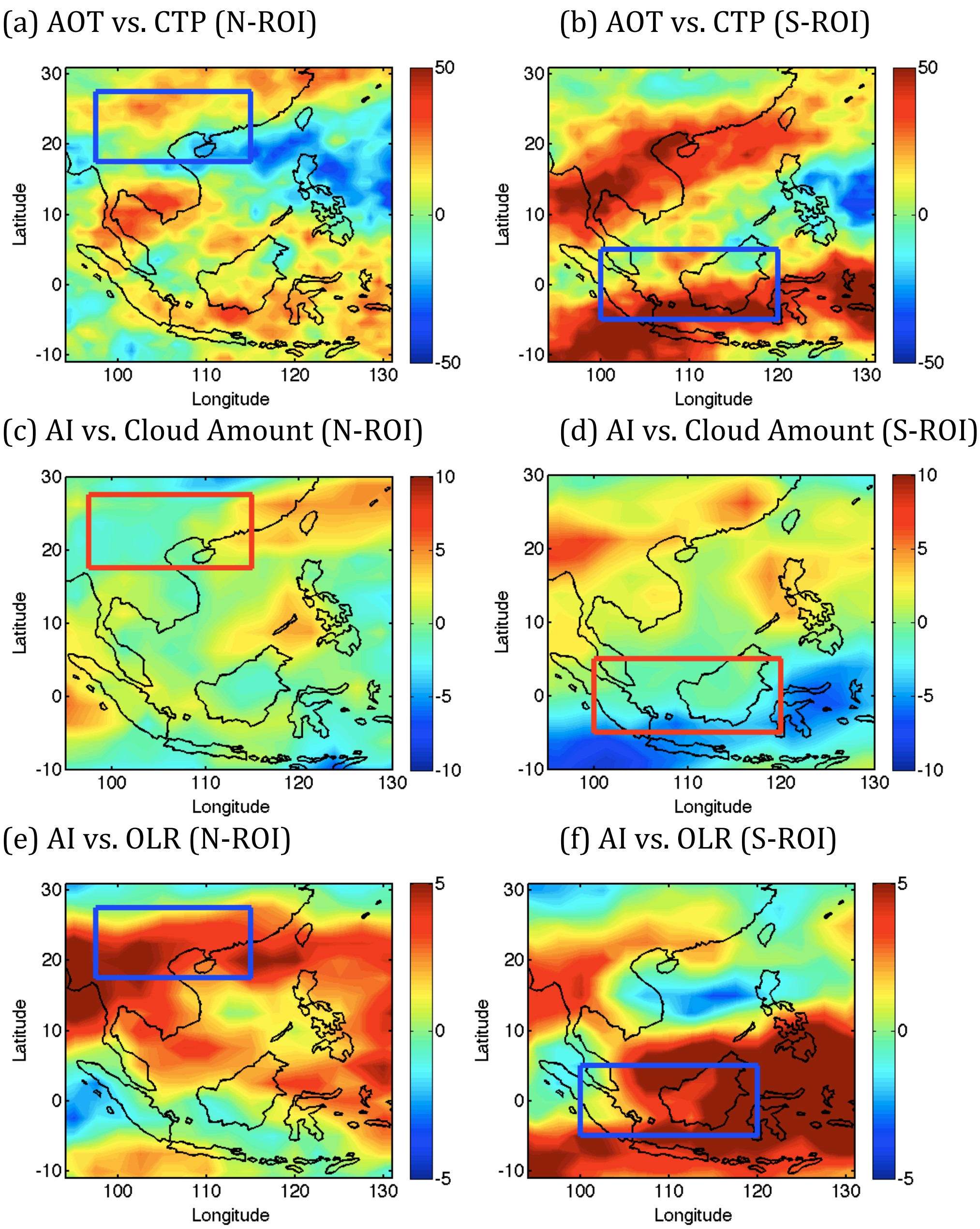

Figure 10. Difference composites of CTP, Cloud Amount and OLR anomalies between high and low aerosol tercile months: (a) CTP over the N-ROI; (b) CTP over the S-ROI; (c) Cloud Amount over the N-ROI; (d) Cloud Amount over the S-ROI; (e) OLR over the N-ROI, and (f) OLOR over the S-ROI.

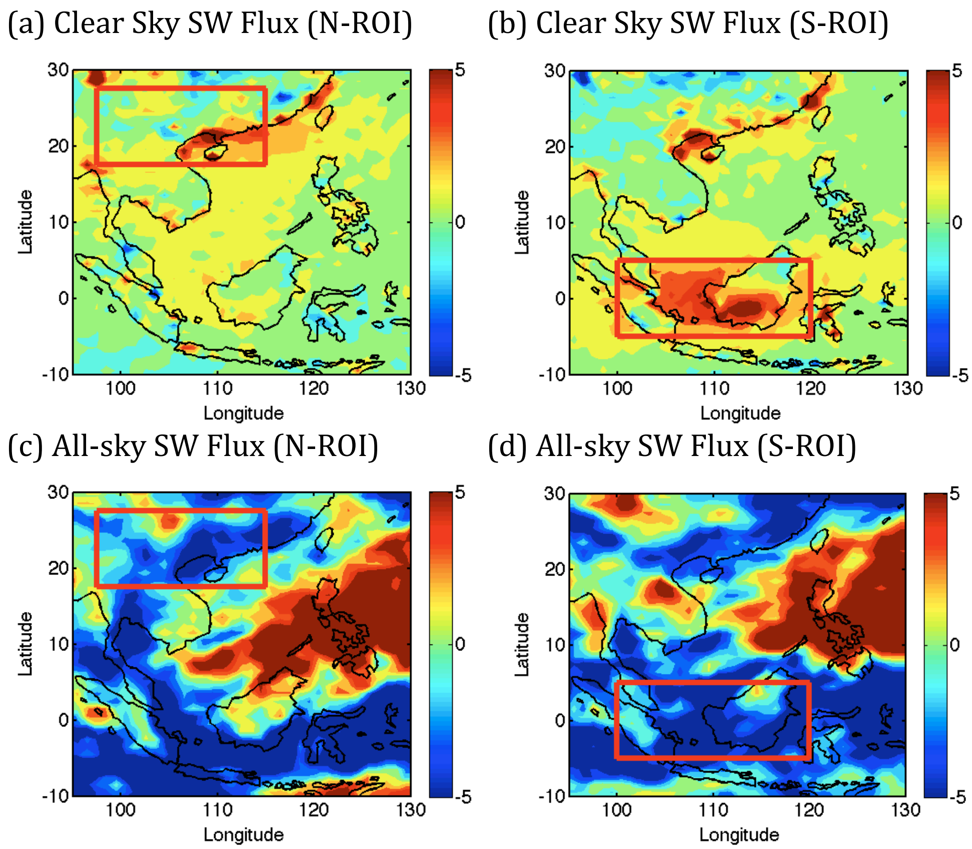

Figure 11. Difference composites of Terra CERES retrieved TOA shortwave flux anomalies between high and low aerosol tercile months in aerosol normalized anomalies: (a) clear sky SW flux over N-ROI; (a) clear sky SW flux over S-ROI; (a) all-sky SW flux over N-ROI; and (d) all-sky SW flux over S-ROI. The unit of the flux is W/m^2.

(a) Low LWP (b) High LWP

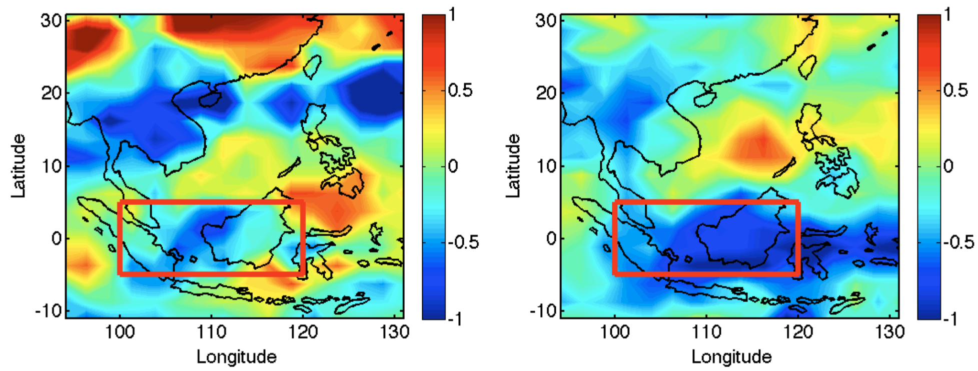

Figure 12. Difference composites of precipitation anomalies between high and low aerosol tercile months over the S-ROI: (a) only for low LWP tercile months; (b) only for high LWP tercile months.

(a) TP (N-ROI, FMA) (b) All-sky SW Flux (N-ROI, FMA) (c) CTP (N-ROI, FMA)

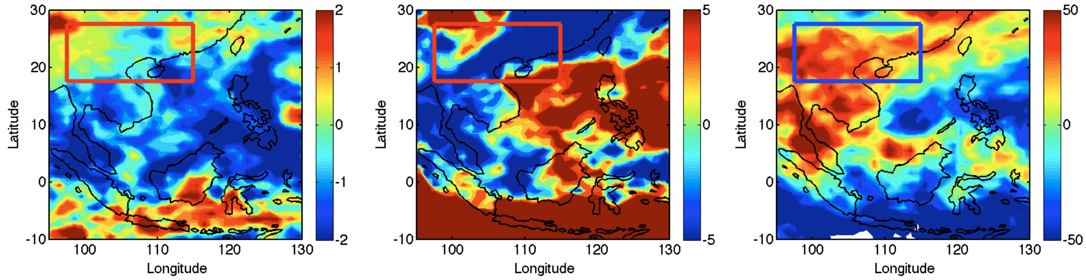

(d) TP (S-ROI, SON) (e) All-sky SW Flux (S-ROI, SON) (f) CTP (S-ROI, SON)

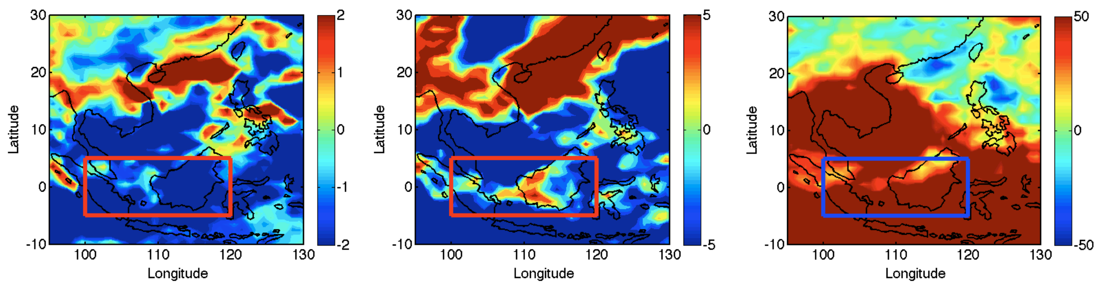

Figure 13. Difference composites of anomalies in (a,d) TRMM precipitation (mm/day), (b,e) CERES All-sky SW flux (K/hour), and (c,f) MODIS Cloud Top Pressure (hPa), over the N-ROI domain between high and low aerosol normalized anomalies tercile months when only data from boreal early spring season (Feb-Mar-Apr) were used in the Top Panel, and over the S-ROI domain between high and low aerosol normalized anomalies tercile months when only data from boreal fall season (Sep-Oct-Nov) were used in the Bottom Panel.